journal of the mechanical behavior of biomedical materials 157 (2024) 106630

Contents lists available at ScienceDirect

Journal of the Mechanical Behavior of Biomedical Materials

journal homepage: www.elsevier.com/locate/jmbbm

Machine learning to mechanically assess 2D and 3D biomimetic electrospun scaffolds for tissue engineering applications: Between the predictability and the interpretability

Elisa Roldán [a,*], Neil D. Reeves [b,c], Glen Cooper [d], Kirstie Andrews [a]

[a] Department of Engineering, Faculty of Science & Engineering, Manchester Metropolitan University, Manchester, M1 5GD, UK
[b] Department of Life Sciences, Faculty of Science & Engineering, Manchester Metropolitan University, Manchester, M1 5GD, UK
[c] Lancaster Medical School, Faculty of Health and Medicine, Lancaster University, Lancaster, LA1 4YW, UK
[d] School of Engineering, University of Manchester, Manchester, M13 9PL, UK

ARTICLE INFO

Keywords:
Machine learning
Decision trees
Electrospinning
PVA
Mechanical characterisation
Tissue engineered implants
Biomimetic scaffolds
Ligament
Human tissue

ABSTRACT

Currently, the use of autografts is the gold standard for the replacement of many damaged biological tissues. However, this practice presents disadvantages that can be mitigated through tissue-engineered implants. The aim of this study is to explore how machine learning can mechanically evaluate 2D and 3D polyvinyl alcohol (PVA) electrospun scaffolds (one twisted filament, 3 twisted filament and 3 twisted/braided filament scaffolds) for their use in different tissue engineering applications. Crosslinked and non-crosslinked scaffolds were fabricated and mechanically characterised, in dry/wet conditions and under longitudinal/transverse loading, using tensile testing. 28 machine learning models (ML) were used to predict the mechanical properties of the scaffolds. 4 exogenous variables (structure, environmental condition, crosslinking and direction of the load) were used to predict 2 endogenous variables (Young's modulus and ultimate tensile strength). ML models were able to identify 6 structures and testing conditions with comparable Young's modulus and ultimate tensile strength to ligamentous tissue, skin tissue, oral and nasal tissue, and renal tissue. This novel study proved that Classification and Regression Trees (CART) models were an innovative and easy to interpret tool to identify biomimetic electrospun structures; however, Cubist and Support Vector Machine (SVM) models were the most accurate, with R^2 of 0.93 and 0.8, to predict the ultimate tensile strength and Young's modulus, respectively. This approach can be implemented to optimise the manufacturing process in different applications.

1. Introduction

The gold standard for surgeries such as Anterior Cruciate Ligament (ACL) replacement, coronary artery bypass graft, treatment for gingival recession or skin transplantation is the use of autologous tissues (Laurencin and Freeman, 2005; Rashid et al., 2008; Kamolz et al., 2022; Webb et al., 2023; Moharamzadeh et al., 2012). However, several disadvantages are associated with this practice, such as donor site morbidity, long rehabilitation time or lack of availability, potentially solved through the implantation of tissue engineered grafts.

There are some premises that a tissue engineered graft should achieve: biocompatibility; appropriate biodegradability rate; porosity; its mechanical behaviour should be comparable to the natural tissue that it would replace (Laurencin and Freeman, 2005; Freeman et al., 2007a); and ideally, it should replicate the morphology of the extracellular matrix tissue in order to promote cell proliferation and imitate mechanical response. In terms of material properties, each biological tissue exhibits different mechanical behaviours. For instance, if the goal is to mimic mechanical behaviour of the natural ACL in the linear region, ACL replacements should have an ultimate tensile stress of approximately 38 MPa (Noyes and Grood, 1976) and a Young's modulus of about 111 MPa (Noyes and Grood, 1976), values observed in the natural ACL; however, for gingival grafts the Young's modulus should be about 37 MPa and the ultimate tensile strength of 3.8 MPa (Choi et al., 2020) and for skin replacements those values should vary between 160-70 MPa and 15–28 MPa respectively depending on the location and testing conditions (Joodaki and Panzer, 2018; Ottenio et al., 2015; Ní Annaidh et al., 2012). To imitate the morphology of the biological tissue, the

* Corresponding author.
E-mail address: Elisa.Roldan-Ciudad@mmu.ac.uk (E. Roldán).

https://doi.org/10.1016/j.jmbbm.2024.106630
Received 23 March 2024; Received in revised form 28 May 2024; Accepted 8 June 2024
Available online 17 June 2024

scaffolds should present the diameter of fibres and filaments between 40 and 150 nm to mimic the collagen fibrils, and between 1 and 20 μm to replicate the collagen fibres of the human soft tissue in the extracellular matrix (ECM) (Shino et al., 1995; Moeller et al., 1995; Bancelin et al., 2014; Strocchi et al., 1996; Roldán et al., 2023a).

The conventional electrospinning process allows the production of a sheet-like network of nanofibres similar to the ECM of soft tissue (Chen et al., 2020a). However, 3D scaffolds promote cell growth, migration, cell-cell interaction and tissue morphogenesis, which are essential factors for cell cycle and tissue performance (Sun et al., 2014). Electrospinning in combination with other manufacturing techniques such as gas foaming (Joshi et al., 2015; Jiang et al., 2015), freeze-drying (Si et al., 2016) and 3D printing (Chen et al., 2019, 2020b) were studied to manufacture 3D scaffolds. Although these studies reported optimum morphology and good cell proliferation on their scaffolds, the majority of them they do not assess the mechanical behaviour. Twisted and braided electrospun scaffolds can mimic the morphology to the ECM of soft tissue (Roldan et al., 2023a), improve the flexibility, bear axial/-shear loads and provide torsion stability (Freeman et al., 2007b), useful characteristics for certain artificial grafts. However, there is a lack of studies involving these kind of electrospun scaffolds to be used in different tissue engineering applications and they are mainly focused on producing tendons (Bosworth et al., 2013; Sensini et al., 2017, 2021) and ligaments (Mouthuy et al., 2015; Rothrauff et al., 2017; Roldán et al., 2024).

Each human tissue is subjected to different environmental and loading conditions that must be taken into account to design and treat the scaffolds. For instance, oral, nasal or vascular tissues are constantly in a wet environment; therefore, degradable scaffolds, such as PVA scaffolds, should be crosslinked to reduce the degradation rate while the tissue is formed, and the scaffolds must behave as the native tissue in wet conditions. Another key aspect is the loading of the tissues, it was demonstrated that some tissues, such as the anterior cruciate ligament, are subjected to multidirectional load (Roldán et al., 2016, 2017), therefore different loading conditions, such as longitudinal or transverse loading, should to be considered to evaluate the final scaffold, which must support the same loading as the native tissue. Therefore, the understanding of how crosslinking and testing conditions (environmental and loading) influence the mechanical behaviour of 2D and 3D structures is crucial, to design and evaluate tissue engineered scaffolds.

Traditional statistical models, such as Multivariate Analysis of Variance (MANOVA) or linear regression models, and Machine Learning (ML) techniques are excellent tools to understand the importance of different factors (exogenous variables) on the predicted variables (endogenous variables). ML models play a key role, providing the highest accuracy predictions even when data presents complicated nonlinear interactions or when the parametric conditions are not met (Bzdok et al., 2018a), minimising the time and cost of experimental work after developing the model (Roldán et al., 2023a). However, some ML models such as KNN, SVM or neural networks are more complicated to interpret than others such as linear regression models, CART or CUBIST models. The ML models learn from the data provided to them, knowing the influence that the input variables have had on obtaining their results will allow us to know the reason for their predictions. A model will be better interpreted if the reasons why its decisions have been made are understood (Miller, 2019). In this research the predictability and the interpretability of the models were studied and discussed to determine the best models able to predict the Young's modulus and ultimate tensile strength and assess their suitability to identify the structure and testing conditions that best mimic a human tissue.

The use of ML models in relation with tissue engineering applications increased exponentially in the last decade, from 9 articles published in 2013 to 130 articles published in 2023 (maximum recorded so far). Such increase is partly due to the recent advances in the ML field as well as the broad availability of ML toolboxes and software packages (Yagli et al., 2019), such as Scikitlearn a Python package (Pedregosa et al., 2011) or the libraries PyCaret (PyCaret Available online) and Caret (Kuhn, 2008) available in Python and R, respectively. Caret library was used in this research due to its simplicity in aspects such as data preprocessing, hyperparameter tuning, and training steps.

However, only three original articles were found that studied the use of ML tools to predict the mechanical behavior of electrospun scaffolds, and only two of them for tissue engineering purposes. Vatankhah et al. used neural networks to predict the Young's modulus of electrospun polycaprolactone/gelatin scaffolds for tissue engineering applications, knowing the manufacturing parameters such as polymer concentrations and rotation speed, and morphological properties such as fibre diameter and alignment of the fibres (Vatankhah et al., 2014). The optimisation of manufacturing parameters such as the concentration of the polymer, flow rate, voltage, type of collector, diameter of the needle, distance between needle and collector and revolutions of the mandrel was explored, with decision trees and neural network, by Roldan et al. to develop electrospun scaffolds with comparable mechanical and morphological properties to human blood vessels (Roldán et al., 2023a). And Muqeet et al. used machine learning models, implemented in PyCaret, to improve the cellulose nanofiber mechanical stability through ionic crosslinking and interpretation of adsorption data for potable water treatment (Muqeet et al., 2023).

The aim of the present study is to explore the suitability of traditional statistical models (Multivariate Analysis of Variance) and 28 machine learning algorithms to predict the mechanical behaviour (ultimate tensile strength and Young's modulus) of 2D and 3D PVA electrospun structures (one twisted filament scaffolds, 3 twisted filaments scaffolds and 3 twisted/braided filaments scaffolds) and assess their suitability to identify the structure that best mimic a specific human tissue. In order to achieve this goal, crosslinked and non-crosslinked 2D and 3D structures, under dry and wet conditions and longitudinal and transversal testing were mechanically analysed to inform the models.

This novel approach allows prediction of combinations of factor levels that can generate biomimetic scaffolds for a wide variety of human tissue replacements. The same methodology can be applied to optimise the manufacturing process across various applications.

2. Materials and methods

2.1. Materials

PVA purchased from Sigma Aldrich (UK) was diluted in distilled water (dH_2O) in a concentration of 12% w/v by heating at 100 °C and stirring for 1 h until a homogenous solution was achieved.

Crosslinked samples were manufactured using 25% glutaraldehyde acquired from Sigma Aldrich (UK).

2.2. Manufacturing process

An electrospinning device (Spraybase®, Ireland) was used to fabricate the electrospun meshes. After an optimization process (Roldán et al., 2023a; Roldan et al., 2023b), a 20 ml syringe was loaded with 10 ml of polymer solution, and it was pumped with a flow rate of 1 ml/h through a 18 G needle. An electrostatic field was created applying high voltage of 20 kV between the tip of the needle and the collector. The fibres were projected from the tip of the needle over a sheet of aluminium foil attached to a 9.65 cm diameter rotating collector working at 2000 rpm. The distance between the needle and the collector was set up to 8 cm. The sheet-like electrospun meshes were manufactured at room temperature (25 °C) and for 3 h spin time (Roldán et al., 2023a, 2023b). A total of 12 sheet-like electrospun meshes were produced in 4 days (3 sheet-like electrospun meshes/day).

2.2.1. Fabrication of the 2D electrospun scaffolds

Both non-crosslinked and crosslinked 2D structures were fabricated by cutting the sheet-like electrospun meshes in a dog-bone shape (25 ×

4 mm, test length x width. Typical thickness of the sheet-like electrospun meshes was 50 μm) in order to test them mechanically and compare their mechanical behaviour to the 3D electrospun structures. A total of 40 2D scaffolds were manufactured, 3 samples per sheet-like electrospun mesh were taken from 10 meshes, and 5 samples per mesh from 2 electrospun meshes.

2.2.2. Fabrication of the 3D electrospun structures

The sheet-like electrospun meshes were cut into rectangles of 2 × 15 cm, carefully peeled from the aluminium foil, and manually twisted clockwise to form a packed filament. Each filament was then cut in half to optimise the sample size to be tested and three different types of scaffolds were created with those filaments: one filament scaffolds, 3 twisted filaments scaffolds and 3 twisted/braided filaments scaffolds. One twisted filament scaffolds were created by manually twisting the sheet-like electrospun scaffolds. 3 twisted filaments scaffolds were fabricated by twisting together three of the one filament scaffolds, the three filaments were twisted together, in a clockwise manner, until a packed and stable structure was created. 3 twisted/braided filaments scaffolds were manufactured by manually braiding three twisted filaments with similar diameters. 90 3D samples were produced, 30 scaffolds per 3D structure. 2 samples of each 3D structure per mesh were manufactured from 10 electrospun meshes, and 5 samples of each 3D structure per mesh from 2 electrospun meshes.

Crosslinked and non-crosslinked scaffolds 3D samples were manufactured following the same procedure described above.

2.3. Crosslinking process

A total of 90 samples were crosslinked by vapour deposition. These samples were placed on a cardboard frame over a metallic mesh in a sealed desiccator and were exposed to 25 ml of 25% glutaraldehyde (GTA) for 24 h, following previous studies (Roldán et al., 2023a, 2023b; Roldan et al., 2023a). After the samples were crosslinked, they were dried under a fume hood for 24 h to reduce the moisture and toxicity of the samples.

2.4. Mechanical characterisation

Tensile tests were performed on non-crosslinked and crosslinked samples of each structure under dry and wet conditions to determine the Young's modulus and the ultimate tensile strength (UTS). Wet samples were immersed in phosphate-buffer saline solution (PBS) for 1 min and tested within the next minute after removal from PBS to maintain the moisture, following previous studies (Roldan et al., 2023a; Roldán et al., 2024). Crosslinked 2D scaffolds were longitudinally and transversally tested in dry conditions. A total of 128 samples were tested (10 samples per combination of structures and conditions) following Table 1.

The 2D and 3D samples were prepared as reported in section 2.2 and placed them separately on cardboard frames to allow the alignment of the sample in the tensometer (Instron H10KS, US). Once the samples were aligned, both sides of the cardboard frame were cut before testing.

To accurately determine the nominal cross-sectional area of each scaffold, the thickness of each sample was measured three times with a digital calliper, an analogue calliper and through SEM images and the average calculated. The limitations of each technique related to the calculus of the nominal cross-sectional area were discussed in the discussion section.

All the mechanical tests were conducted under the same conditions: at room temperature (25 °C), with a 100 N load cell, 5 mm/min test speed and rubber pneumatic clamps to reduce stress concentrations (Roldan et al., 2023a). However, a preload of 0.1N was applied in wet samples to fully align them in the tensometer.

2.5. Mechanical requirements for tissue engineered grafts

Mechanical properties of common human tissue previously reported (Roldán et al., 2023b) were used to benchmark the experimental results of the present study and assess the possibility of using certain structures in different environmental/loading conditions for a variety of tissue engineered grafts. This identification was carried out traditionally, with the mean and standard error of the mechanical properties of each manufactured scaffold, and through CART models to predict the Young's modulus and the ultimate tensile strength. The results of both techniques were discussed in this research.

2.6. Statistical analysis

An initial exploratory analysis and a treatment of aberrant data were conducted prior to developing the models.

The normality and homoscedasticity were assessed through Kolmogorov Smirnov and Breusch-Pagan tests respectively.

Traditional statistical approaches, such as Multivariate Analysis of Variance (MANOVA), were conducted to be compared with machine learning models and evaluate the significance of the independent variables (structure, environmental condition, crosslinking and direction of the load) and their interactions on the dependent continuous variables (Young's modulus and ultimate tensile strength). The accuracy of these models was assessed by the coefficient of determination. Partial squared Eta values were used to determine the effect sizes produced by endogenous variables, factors and interactions (Roldán et al., 2023a, 2023b).

To identify which manufactured scaffold could be suitable to replace a specific human tissue in a traditional manner, the mean and standard deviation (Std Dev) were calculated for each mechanical property for all 2D and 3D structures and conditions.

Descriptive statistics of all the predictions obtained with RF, KNN, CUBIST and SVM were used to assess which model could get a better approximation to certain human tissue.

SPSS version 29.0.1.0 (IBM Inc, US) was used to conduct all statistical analyses, descriptive and exploratory and inference analysis.

Table 1
Design factors and number of samples per factor.

	Structure	Environmental condition	Crosslinked	Orientation	Number of Samples
Our Scaffolds	**2D**	Dry	Non-Crosslinked	Longitudinal	10
			Crosslinked	Longitudinal	10
				Transverse	10
		Wet	Crosslinked	Longitudinal	10
	3D 1 Filament	Dry	Non-Crosslinked	Longitudinal	10
			Crosslinked	Longitudinal	10
		Wet	Crosslinked	Longitudinal	10
	3D 3 twisted filaments	Dry	Non-Crosslinked	Longitudinal	10
			Crosslinked	Longitudinal	10
		Wet	Crosslinked	Longitudinal	10
	3D 3 twisted/braided filaments	Dry	Non-Crosslinked	Longitudinal	8
			Crosslinked	Longitudinal	10
		Wet	Crosslinked	Longitudinal	10

2.7. Machine learning models

2.7.1. Predictability

A total of 28 ML models were studied in this research. 4 exogenous variables (structure, environmental condition, crosslinking and direction of the load for 2D scaffolds) were used to predict 2 endogenous variables (Young's modulus and ultimate tensile strength). 128 observations for each endogenous variable informed a Multivariate Analysis of Variance (MANOVA) whose results were compared to the results obtained with 28 parametric and non-parametric machine learning (ML) models, including Linear Models (LM), Generalized Linear Model (GLM), Generalized Additive Model (GAM), Stepwise Model Selection by Akaike information criterion (Step AIC), Multivariate Adaptive Regression Splines (MARS, also known as EARTH models), Lasso and Elastic-Net Regularized Generalized Linear Models (GLMNET), Support Vector Machine (SVM), Tune SVM (optimised SVM), Classification and Regression Trees (CART), k-Nearest Neighbours (KNN), Random Forest (RF), Generalized Boosted Regression Models (GBM), cubist models (CUBITS) and Tune CUBIST (optimised CUBIST), to select the most accurate model for each dependent variable.

Linear models were used in this study for comparison purposes with the rest of the ML models following previous research (Roldán et al., 2023a).

For all of the models the pre-processes were set up as "center", "scale" and "BoxCox". All models were validated with a nested cross-validation (Fig. 1). The outer loop corresponded to a leave-one day-out 4 folds cross-validation (1 fold per day). The test data of the outer loop included scaffolds created from 3 sheet-like meshes manufactured the same day. Training data of the outer loop included the scaffolds manufactured from 9 sheet-like scaffolds created in different days that the scaffolds included in the test data. Inner loops of 10-folds cross-validation and 3 repeats were created with the function "trainControl ()" and the method "repeatedcv", to optimise the hyperparameters of models such as Cubist and SVM through the function "expand.grid()". Sigma values of 0.025, 0.05, 0.1, 0.15 and a sequence between 1 and 10 were used to optimise the hyperparameters of SVM models (Tune SVM). To optimise hyperparameters for CUBIST models (Tune CUB) committees with sequences between 15 and 25 and K-neighbours of 3, 5, and 7 were evaluated. The default hyperparameters and settings embedded in the "caret()" library were used for the rest of the models.

Final R^2 and Mean Absolute Percentage Error (MAPE) and Root Mean Square Error (RMSE) of the cross-validation (R^2_{CV}, $MAPE_{CV}$ and $RMSE_{CV}$) were calculated with the average of the results of these parameters obtained per day ($R^2_{CV\_day1}$ until $R^2_{CV\_day4}$, $MAPE_{CV\_day1}$ until $MAPE_{CV\_day4}$ and $RMSE_{CV\_day1}$ until $RMSE_{CV\_day4}$), which were calculated with the average of the R^2, MAPE and RMSE results for each validation stage (R^2_{CV1} until R^2_{CV10}, $MAPE_{CV1}$ until $MAPE_{CV10}$ and $RMSE_{CV1}$ until $RMSE_{CV10}$).

The different data sets are represented in Fig. 1.

To determine the most accurate model per independent variable, the final MAPE and RMSE errors ($MAPE_{Test}$ and $RMSE_{Test}$), and the fitted values of R^2 (R^2_{Test}) were calculated with the average of the results obtained per day with test data (R^2_{Test1} until R^2_{Test4}, $MAPE_{Test1}$ until $MAPE_{Test4}$ and $RMSE_{Test1}$ until $RMSE_{Test4}$) and the "predict()" function.

The importance of the exogenous variables on the endogenous variables was calculated, for all the ML models, with the function "varImp ()" and training and validation data. A percentual average of the importance of the variables was calculated considering all popular ML models (14 models per independent variable), all the scaffolds created per day (4 days) and all the repetitions for the cross-validation (30 repetitions per day). Therefore, the importance of the predictors on the predicted variable was computed with a total of 1680 cases per independent variable (Young's modulus and ultimate tensile strength).

All the models and functions used in this research are implemented in the library "caret()" of R-4.3.2 and RStudio 2023.10.31.

2.7.2. Interpretability

Regression coefficients of LM, GAM, EARTH and Step AIC models were obtained with the function summary(). This function also provides standard errors, significance level (P value), R^2 and AIC (Akaike information criterion) to determine the best predicted model penalising complex models to avoid overfitting. The interpretation of linear models is the easiest since the regression coefficients allows to create a mathematical relationship between the dependent and the independent variables (equation (1)).

$$E \text{ or } UTS = intercept + 1TF, 3TF, 3TBF\ structure + \beta_1\ condition + \beta_2\ crosslinking + \beta_3\ direction \quad (1)$$

Where β_1, β_2 and β_3 are the regression coefficients of each exogenous variable, condition would be 0 for dry samples and 1 for wet samples, crosslinking would be 0 for non-crosslinked samples and 1 for crosslinked samples, direction would be 0 for longitudinal and 1 for transverse, and structure would be 0 for 2D structures and 1 for any 3D structure. The regression coefficients for the structure will depend on the structure, coefficients 1TF correspond to 1 filament scaffolds, 3TF coefficient will be applicable for just 3 twisted filament scaffolds and 3TBF are the coefficients applied to 3 twisted/braided filament scaffolds.

CART models are non-parametric supervised learning algorithms and were selected due to their easy interpretability. Two inverted trees were created in this research to present the predictions and importance of the independent variables on the prediction of the dependent variables

Fig. 1. Validation process of the model.

(Young's modulus and ultimate tensile strength). These models can be pruned to enhance their interpretability; however, the prune function was not used to favour the identification of the structure that under an environmental and loading condition would be suitable as human tissue replacement. For this goal, the terminal leaf and the path followed to reach that leaf was considered, and the mean and standard deviation of the predicted dependent variable (Young's modulus or ultimate tensile strength) were graphically compared with the same property for the different human tissues obtained in a previous research (Roldán et al., 2023b).

CUBIST models provide an effective model interpretability while offering powerful predictive performance. These models are based on decision trees with series of "if-then" rules in their branches which are associated with a multivariate linear regression model in the terminal leaf. CUBIST models add boosting with training committees and K nearest neighbours to adjust the predictions generated by the model rules (Kuhn et al., 2014; Kuhn and Johnson, 2013). The function summary() provided all the rules and multivariate linear regressions, which offered an easier understanding than other ML techniques such as SVM or KNN while giving a better predictions than simple techniques such as multivariate linear regression.

SVM is a powerful non-parametric supervised machine learning technique used for classification, regression and outliers detection (Smola and Schölkopf, 2004). A linear score classifier is provided by SVM; however, the coefficient function that defines that linear score exhibits many irregular oscillations which makes difficult its interpretation (Martin-Barragan et al., 2014).

The KNN method can be used for regression and classification and uses the nearest neighbours (or the average of the neighbours, in case of regression) of a data point for prediction. The interpretation of this method is tricky mainly for two reasons; first, there is no interpretability on a modular level due to no parameters are used to learn; second, there are not global weights or structures explicitly learned and therefore its global interpretability is complicated. The interpretability of this method will highly depend on the data set, being more uninterpretable as many features we have to create the model (Molnar, 2019).

Due to the demonstrated similarity of the errors and R^2 calculated with test data and after the cross-validation, we used the descriptive statistics of all predictions of the Young's modulus and UTS for each structure and testing conditions obtained with RF, KNN, SVM and CUBIST models and we compared the different factor's levels to human tissues to identify the most suitable structure for human tissue replacement.

3. Results

3.1. Statistical analysis

After an initial exploratory analysis and a treatment of aberrant data, two of the mechanical values observed for 3 twisted/braided filaments scaffolds resulted in aberrant values and were considered out of the study.

Kolmogorov Smirnov and Breusch-Pagan tests proved that none of the 2 output variables followed a normal distribution (P value < 0.001), and they did not meet the homoscedasticity (P value < 0.001). Therefore, popular statistics models such as general linear models or Multivariate Analysis of Variance (MANOVA) models would be not suitable for this study. Nonetheless, these approaches were included in this research due to their popularity in the scientific community, and their accuracy and importance (Eta values) of each exogenous variable were discussed and compared to those of machine learning models. Table 2 presents the MANOVA for the Young's modulus and ultimate tensile strength, Fisher's number, significance, Eta value and coefficient of determination (R^2).

MANOVA analysis presented significant differences for the Young's modulus and ultimate tensile stress (P value < 0.0001) depending on scaffold structure, environmental condition (dry or wet samples), testing direction (longitudinal or transversal to the fibres) and structure/environmental condition interactions. Also, crosslinked and non-crosslinked samples exhibited significant differences (P value < 0.0001) for ultimate tensile stress; however, they presented borderline significant differences (P value $= 0.046$) in Young's modulus. No significant differences were observed in both Young's modulus and ultimate tensile stress for the interaction between crosslinked and structure (P value $= 0.263$ and P value $= 0.272$ respectively).

Table 2
MANOVA for the Young's modulus and ultimate tensile strength.

Intersubject effects test				
Origen	Dependent variable	F	Sig.	Eta partial squared
Corrected model	Young's Modulus	42.681	0.000	0.817 [a]
	Ultimate tensile strength	33.271	0.000	0.776 [b]
Intersection	Young's Modulus	742.796	0.000	0.866
	Ultimate tensile strength	1356.070	0.000	0.922
Structure	Young's Modulus	64.408	0.000	0.627
	Ultimate tensile strength	56.198	0.000	0.594
Environmental condition	Young's Modulus	196.665	0.000	0.631
	Ultimate tensile strength	122.039	0.000	0.515
Direction	Young's Modulus	141.620	0.000	0.552
	Ultimate tensile strength	50.297	0.000	0.304
Crosslinked	Young's Modulus	3.969	0.049	0.033
	Ultimate tensile strength	13.098	0.000	0.102
Structure * Condition	Young's Modulus	20.371	0.000	0.347
	Ultimate tensile strength	11.920	0.000	0.237
Structure * Crosslinked	Young's Modulus	1.347	0.263	0.034
	Ultimate tensile strength	1.318	0.272	0.033

[a] $R^2 = 0.817$ (Young's Modulus).
[b] $R^2 = 0.776$ (Ultimate tensile strength).

Eta values were studied to evaluate the importance of the independent variables on the dependent variables (Table 2). Eta values of 0.627, 0.631depend and 0.552 were obtained for the influence of the structure, the environmental condition (dry vs. wet samples) and the loading direction on the Young's modulus, demonstrating a high importance of these independent variables on this dependent variable. It was also observed that the structure and environmental condition (dry vs. wet samples) highly affected the ultimate tensile stress exhibiting Eta values of 0.594 and 0.515.

Fig. 2 shows the MANOVA predicted values vs. the observed values for both mechanical properties.

Traditionally, the way to identify which structure would mechanically behave more similarly to a specific tissue, would be through the mean and standard deviation of specific mechanical properties. Table 3 presents the mean and Std Deviation of the Young's modulus and ultimate tensile strength for each structure and manufacturing and testing condition, and they are compared with biological human tissue in the same range.

3.2. Machine learning models

3.2.1. Predictability

Although R^2 informs us of the goodness of fit of the model, this does not mean that all of those who have high or low R^2 are good or bad models; the combination of the study of the coefficient of determination and the accuracy of the model, defined by the type of errors, will be decisive. To select the most accurate model, graphical interpretations of the coefficient of determination and precision parameters (MAPE and

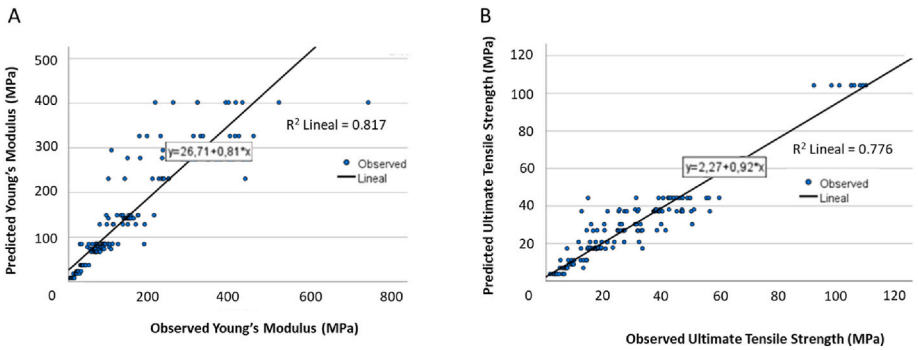

Fig. 2. MANOVA predicted values vs. the observed values A) Young's modulus and B) ultimate tensile strength.

Table 3
Comparative between mechanical properties of our scaffolds and human tissues (Mean ± Std Dev).

					Young's Modulus (MPa)	Ultimate Tensile Strength (MPa)	References
Our Scaffolds	**2D**	Dry	Non-Crosslinked	Longitudinal	326.7 ± 100.1	27.1 ± 8.6	
			Crosslinked	Longitudinal	401.7 ± 149.8	30.3 ± 9.8	
				Transverse	67.8 ± 6.3	7.1 ± 2.2	
		Wet	Crosslinked	Longitudinal	37.6 ± 6.4	3.8 ± 1.5	
	3D 1 Filament	Dry	Non-Crosslinked	Longitudinal	277.2 ± 74.4	37.2 ± 9.6	
			Crosslinked	Longitudinal	333.7 ± 157.4	54.4 ± 35.6	
		Wet	Crosslinked	Longitudinal	73.9 ± 15.6	37.2 ± 12.1	
	3D 3 twisted filaments	Dry	Non-Crosslinked	Longitudinal	85.4 ± 12.8	17.9 ± 2.3	
			Crosslinked	Longitudinal	84.9 ± 47.3	20.9 ± 5.9	
		Wet	Crosslinked	Longitudinal	8.5 ± 3.9	11.3 ± 3.2	
	3D 3 twisted/braided filaments	Dry	Non-Crosslinked	Longitudinal	128.9 ± 37.5	26.9 ± 5.4	
			Crosslinked	Longitudinal	149.3 ± 32.6	38.2 ± 7.6	
		Wet	Crosslinked	Longitudinal	23.7 ± 2.9	9.0 ± 0.4	
Skin tissue					83.3 ± 34.9	21.6 ± 8.4	Ní Annaidh et al., 2012
	Parallel to the fibres				160.8 ± 53.2	28.0 ± 5.7	Ottenio et al., 2015
	Perpendicular to the fibres				70.6 ± 59.5	15.6 ± 5.2	Ottenio et al., 2015
	Middle back parallel to the fibres				112.5	17–28	Ní Annaidh et al., 2012; Joodaki and Panzer, 2018
Connective tissue	**Anterior cruciate ligament**				111	38	Noyes and Grood, 1976
Other tissue	**Nasal periosteum**					3.88	Zeng et al., 2003
	Gingiva				37.36 ± 17.4	3.81 ± 0.9	Choi et al., 2020

RMSE) have been used.

Fig. 3 shows the MAPE and R^2 of each ML model to predict the Young's modulus and ultimate tensile strength. Both, MAPE and coefficient of determination were calculated with test data. Fig. 3A shows the coefficient of determination and MAPE for each ML regression model used to predict the Youngs modulus, whereas Fig. 3B indicates the MAPE and goodness of fit of each model to predict the ultimate tensile strength.

From the above figure (Fig. 3) and as expected, we observed a clear trend between R^2 and MAPE, as higher the R^2 was, lower MAPE we obtained for the models, and as lower R^2, higher MAPE was observed. This trend is obvious for almost all models predicting both Young's modulus and ultimate tensile strength. However, models such as LM, GLM, step AIC and GLMNET presented worst R^2 than the GAM and EARTH models, but these last models exhibited MAPE errors higher than the others. The inflection point between good and bad models was observed from CART models, where R^2 started increasing whereas MAPE started decreasing.

CUBIST, SVM and RF models were the best models with values of R^2

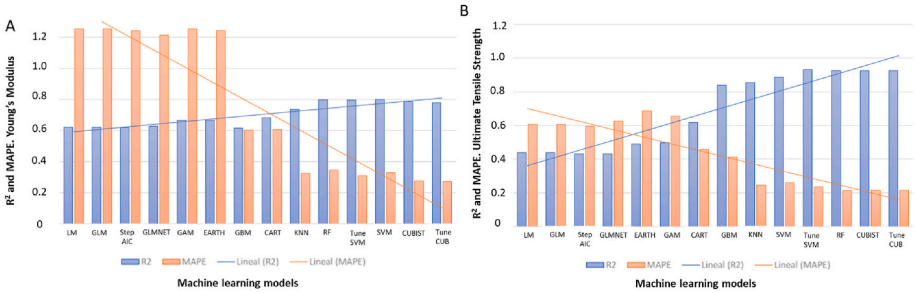

Fig. 3. R^2 and MAPE of each model to predict with test data A) Young's modulus and B) Ultimate Tensile Strength.

of 0.8 and 0.93, and MAPE of 0.27 and 0.21, for Young's modulus and ultimate tensile strength respectively.

The comparative between R^2 and RMSE obtained with the cross-validation and with test data for each model to predict the Young's modulus and ultimate tensile strength are shown in Fig. 4. Once the models were organised following their R^2 and RMSE the trendlines were added to check the convergency between the results calculated from test data or after cross-validation.

Fig. 4A represents the coefficient of determination for the models predicting the Young's modulus calculated from test data and cross-validation data. This graph shows that the best models Tune CUB (optimised CUBIST), CUBIST, Tune SVM, RF and SVM tended to converge to R^2 of 0.8 with values of coefficient of determination calculated from test data slightly lower than the values after cross-validation. The RMSE errors predicting the Young's modulus calculated from test data were lower than the RMSE calculated after cross-validation (Fig. 4C). Fig. 4B shows that R^2 reached 0.93 for CUBIST, RF and Tune SVM calculated from test data, these results were surpassing better than the results obtained from cross-validation. Fig. 4D shows an improvement of RMSE calculated for test data versus cross-validation for the best models mentioned above and predicting the ultimate tensile strength. All these results corroborated the same as was shown in Fig. 3, the best models to predict the Young's modulus and ultimate tensile strength were the CUBIST models, RF and SVM models, and the fact that the best accurate models had better predictions with test data than after cross-validation, confirmed the replicability and reproducibility of the method.

The importance of each factor and their levels, that have the greatest participation in shaping its predictions, were found for the 14 ML models.

The structure factor has the greatest participation in the prediction of the Young's modulus of the scaffolds, with a 50% of the total importance due to this factor. Dry/wet testing conditions experienced an importance of 32%. Surprisingly, testing direction (longitudinal/transverse) and the effect of crosslink the scaffold (non-crosslinked/crosslinked) exhibited a low influence on the prediction of this endogenous variable with 17% and 1% respectively. For the prediction of the ultimate tensile strength, the variable with the highest importance was condition (43%), followed by direction (36%), structure (12%) and crosslinking (9%).

Analysing the factor levels more in detailed, it was observed that the wet condition along with the 3D 3 twisted/braided filaments structure contributed the most to the mechanical properties of the scaffolds. Fig. 5

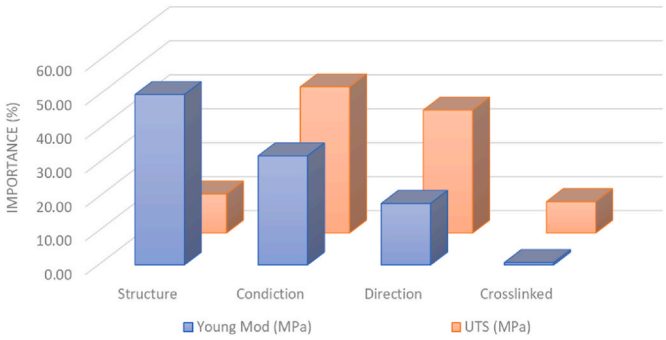

Fig. 5. Importance of independent variables in the prediction of the dependent variables.

shows the importance of each independent variable in the prediction of the Young's modulus and ultimate tensile strength.

3.2.2. *Interpretability*

A ML model should be as much reliable and robust as possible, where smalls changes do not highly affect the predictions. To understand how the independent variables affect the predictions, it is important to be able to interpret the model (Doshi-Velez and Kim, 2017). Intrinsic methods of interpretation of a ML model provide statistical summaries, graphs or regression coefficients/weights to understand how the exogenous variables influence the endogenous variables. Some intrinsic interpretable models are LM, GAM, EARTH, Step AIC, CART or CUBIST (Molnar, 2019; Ribeiro et al., 2016).

Table 4 shows this regression coefficients/weights to predict the Young's modulus and ultimate tensile strength for LM, Step AIC, GAM and EARTH models. Regression coefficients determine the weight of each factor level on the predicted variable.

The weights and intercepts calculated for the LM, StepAIC, GAM, and EARTH models are very similar in value and with identical degrees of significance.

Analysing the regression coefficients and intercept calculated to predict the Young's modulus, it is observed that all the coefficients related to the structure were negative, contributing more negatively to the Young's modulus the 3 twisted/braided filaments structure. 2D structure did not experience any influence on the predicted variables, as it was set up as zero, and therefore, the predictions for this structure did

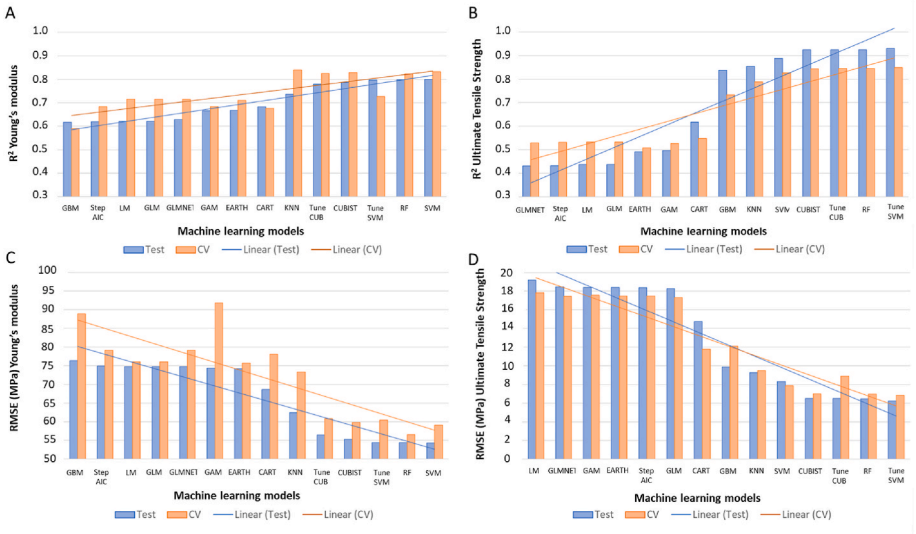

Fig. 4. Comparative between R^2 and RMSE calculated from test data and with cross-validation with each model A) R^2 to predict Young's modulus, B) R^2 to predict Ultimate Tensile Strength, C) RMSE to predict Young's modulus and D) RMSE to predict Ultimate Tensile Strength.

Table 4
Regression coefficients/weights to predict the Young's modulus and ultimate tensile strength through LM, Step AIC, GAM and EARTH models.

Coefficients		LM		StepAIC		GAM		EARTH	
Young's modulus (MPa)	**Intercept**	154.07	***	154.07	***	154.07	***	154.07	***
	Structure: 1TF	−22.90	*	−22.90	*	−22.90	*	−24.16	*
	Structure: 3TF	−61.09	***	−61.09	***	−61.09	***	−61.68	***
	Structure: 3TBF	−89.33	***	−89.33	***	−89.33	***	−89.99	***
	Condition: Wet (r_1)	−78.33	***	−78.33	***	−78.33	***	−74.25	***
	Crosslinking: Yes (r_2)	14.73		14.73		14.73		0.00	
	Direction: Transverse (r_3)	−93.98	***	−93.98	***	−93.98	***	−86.64	***
UTS (MPa)	**Intercept**	23.86	***	23.86	***	23.86	***	23.86	***
	Structure: 1TF	8.73	***	8.73	***	8.73	***	8.64	***
	Structure: 3TF	1.20		1.20		1.20			
	Structure: 3TBF	−0.89				−0.89			
	Condition: Wet (r_1)	−5.79	***	−5.49	***	−5.79	***	−5.84	*
	Crosslinking: Yes (r_2)	3.27	**	3.21	**	3.27	**	3.33	
	Direction: Transverse (r_3)	−8.05	***	−8.07	***	−8.05	***	−8.09	***

Significance codes: 0 '***' 0,001 '**' 0,01 '*' 0,05 ',' 0,1 ' '

not decrease the value of the intersect. Furthermore, the structure levels were highly significant (***) with P values less than 0.001 for 3 twisted filaments and 3 twisted/braided filaments structures. The variable environmental condition (dry/wet samples) was highly significant and exerted a high negative influence on the Young's modulus, with a regression coefficient of −78.33 for LM, for wet samples. The crosslinking process did not significantly influence the prediction of the Young's modulus. However, the testing direction had a negative impact on the prediction of the Young's modulus (with a regression coefficient of −93.98 for the LM model) for samples tested transversally to the fibres.

Young's modulus can be predicted with LM for 2D structures, one filament structure, 3 twisted filament structures and 3 twisted/braided filament structures as indicated in equations (2)–(5) respectively.

$$E\,(MPa) = 154.07 - 78.33\ condition + 14.73\ crosslinking - 93.98\ direction \quad (2)$$

$$E\,(MPa) = 154.07 - 22.90\ structure - 78.33\ condition + 14.73\ crosslinking - 93.98\ direction \quad (3)$$

$$E\,(MPa) = 154.07 - 61.09\ structure - 78.33\ condition + 14.73\ crosslinking - 93.98\ direction \quad (4)$$

$$E\,(MPa) = 154.07 - 89.33\ structure - 78.33\ condition + 14.73\ crosslinking - 93.98\ direction \quad (5)$$

As an example, if we want to predict the Young's modulus for a crosslinked 3 twisted filaments structure under tensile test and wet conditions, the equation to apply for LM would be the equation number 5. Substituting all the values as indicated in section 2.8.2, we would get a value of Young's modulus of 13.73 MPa comparable to the 8.5 ± 3.9 MPa obtained from the experimental work.

One filament structure had a highly significant positive regression coefficient of 8.73 in predicting the ultimate tensile strength using a LM. The regression coefficients for 3 twisted filaments structures and 3 twisted/braided filament structures were not significant and 2D scaffolds did not contribute to the predicted variables. The environmental condition (wet samples) had a significant negative effect on the ultimate tensile strength for these models. The crosslinking process significantly affected the ultimate tensile strength prediction, but their significance level was lower than the condition. Direction of the test contributed negatively and significantly to the UTS prediction.

Ultimate tensile strength can be predicted as indicated for the Young's modulus. As an example, the estimated ultimate tensile strength for a crosslinked 2D structure under tensile and longitudinal test and dry conditions with a LM would be 27.13 MPa comparable to the 30.3 ± 9.8 MPa obtained from the experimental work.

Regression coefficients calculated from LM, Step AIC, GAM and EARTH models agreed with the importance of the variables obtained with the average of the importance of all the ML models and the Eta values calculated with the MANOVA.

Even though LM, Step AIC, GAM and EARTH models are easy to interpret, their predictions were not as reliable as other ML techniques, presenting low values of R^2 and high errors. Moreover, LM would be not suitable due to our data did not meet the parametric conditions of a gaussian distribution.

CART models provided better accuracy than the models studied above, and their predictions and importance of the variables are visible and easy to interpret. Fig. 6 shows the CART to predict the Young's modulus.

As shown in Fig. 6, the environmental condition variable was the most important variable to predict the Young's modulus and divides all observations into dry and wet, with a mean of approximately 203 MPa and 36 MPa respectively. Following the incidence of the factors in the graph, 2D and 1 twisted filament structures exhibited higher Young's modulus than the other two structures. It was also observed that the texting direction in dry 2D samples influenced the prediction of the Young's modulus, increasing its value when the samples are tested longitudinally to the fibres and decreasing it when they are tested transversely to the fibres. All these findings were in agreement with the regression coefficient calculated for LM, Step AIC, GAM and EARTH models, the Eta values calculated with the MANOVA and the average of the importance calculated with all the ML models.

Fig. 7 shows the CART to predict the ultimate tensile strength.

In this case, the structure was the most important variable to predict the ultimate tensile strength, with higher predicted values of ultimate tensile strength for the structures 1 twisted filament than 2D structures, 3 twisted filament structures and 3 twisted/braided filament structures. The observations with higher ultimate tensile strength (1 twisted filament) are divided by crosslinked factor into non-crosslinked and crosslinked, with means of UTS of 37.197 MPa and 40.777 MPa respectively. The observations with lower ultimate tensile strength (2D, 3 twisted filament structures and 3 twisted/braided filament structures) are divided by the environmental condition factor, with means of UTS of approximately 23.960 MPa for dry samples and 8.008 MPa for wet samples.

CART models provide a visual and intuitive graph with the predictions and the importance of the variables involved in the model. Observing the paths/branches to reach a terminal leaf we can obtain the predictions of our dependent variables without the necessity of performing any mathematical operation. Fig. 8 compares the predicted mechanical properties obtained through CART models and the mechanical properties of human tissues obtained in a previous study (Roldán et al., 2023b).

CART models identify six different structures tested under different

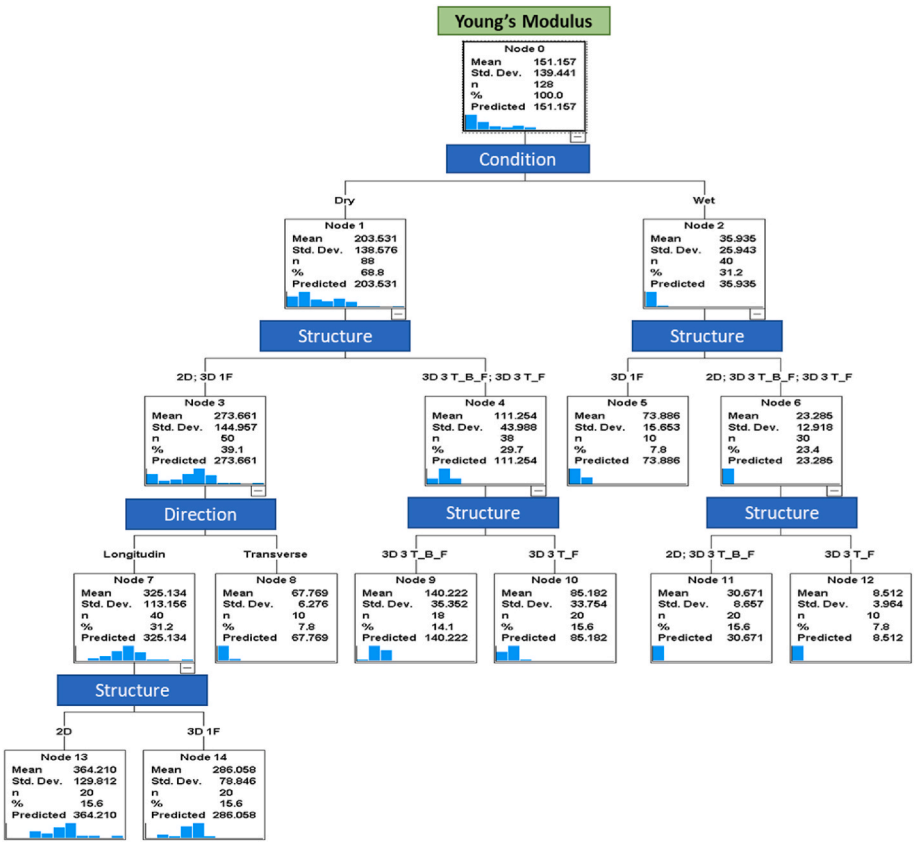

Fig. 6. CART for Young's modulus.

conditions as mechanically suitable to be used as scaffolds for tissue engineering applications such as ligamentous tissue, skin tissue, oral and nasal tissue and renal tissue. 2D wet crosslinked scaffolds under tensile force exhibited a Young's modulus in the same range as human kidney tissue (41.5 MPa (Snedeker et al., 2005)). Dry 3 twisted filament scaffolds under tensile force exhibited Young's modulus similar to the native anterior cruciate ligament (111 MPa (Noyes and Grood, 1976)); however, dry 3 twisted/braided filament scaffolds under tensile testing fully mimicked the mechanical behaviour of the anterior cruciate ligament in terms of Young's modulus and ultimate tensile strength (111 MPa and 38 MPa respectively (Noyes and Grood, 1976)). The mechanical behaviour of human gingiva and human nasal periosteum can be mimicked with 2D wet crosslinked scaffolds under tensile force (Young's modulus of 37.36 ± 17.4 MPa was observed in gingiva (Choi et al., 2020) and UTS of 3.81 ± 0.9 and 3.88 MPa was observed in gingiva and nasal periosteum tissue respectively (Choi et al., 2020; Zeng et al., 2003)). Dry 3 twisted filament scaffolds under tensile force exhibited Young's modulus and UTS in the same range as the human skin tested perpendicular to the fibres (70.6 ± 59.5 MPa and 15.6 ± 5.2 MPa respectively (Ottenio et al., 2015)), whereas dry 3 twisted/braided filaments scaffolds tested under tensile force presented mechanical properties comparable to the human skin tested parallel to the fibres (160.8 ± 53.2 MPa and 28.0 ± 5.7 MPa for Young's modulus and UTS respectively (Ottenio et al., 2015)). All these structures and tissues were also identified as mechanically suitable in Table 3, demonstrating that CART predictions are in the same range as means and standard errors of the mean of each structure and testing condition observed.

CUBIST model established 20 sub-models with a different number of if-then rules on them to predict the Young's modulus. However, only one sub-model with 4 rules was established to predict the ultimate tensile strength. These if-then rules were associated to different observations with different mean and range of the dependent variable, and a multiple regression equation was provided for each rule. The rules were arranged in an ascendant order for the exogenous variable mean, as an example to predict the Young's modulus, the first rule involved observations with a mean of 34.9 MPa whereas the fourth had a mean of 249 MPa. Due to the length and complexity of the sub-models and rules, they are not included in the present article but can be found in the Supplementary Material. Although CUBIST models can be interpreted through the rules and regression equations, they are not as clear as CART models, however the descriptive statistic of their predictions for each structure and testing condition were calculated to identify human tissues with similar mechanical properties as our scaffolds (Table 5).

Table 5 shows the predictions of Young's modulus and UTS obtained with KNN, RF, CUBIST and SVM models for each structure and tensile conditions comparable to human tissues. KNN, RF, CUBIST and SVM models identified the same six tissues presented above with means comparable to the means observed in the experiments in Fig. 3 and with the decision trees' predictions.

All the six ML models evaluated in Table 5, predicted Young's modulus and UTS within the range observed for skin tested parallel to the skin fibres with scaffolds created from 3 twisted/braided filaments with a crosslinked treatment and tensile tested in dry conditions. The mechanical behaviour of skin tested perpendicular to the skin fibres can be also achieved with non-crosslinked 3 twisted filaments scaffolds tested under tensile force in dry conditions. Predictions obtained with crosslinked 3 twisted/braided filaments scaffolds under tensile test in dry conditions were in the same range as the UTS observed for the anterior cruciate ligament but with slightly higher Young's modulus. All the predictions of the UTS obtained with crosslinked 2D scaffolds tested under wet conditions were able to be in the same range of the UTS of the nasal periosteum and gingiva except for the SMV model, whose values were slightly higher than those of human tissues. Prediction of Young's modulus within the range of kidney tissue were obtained with

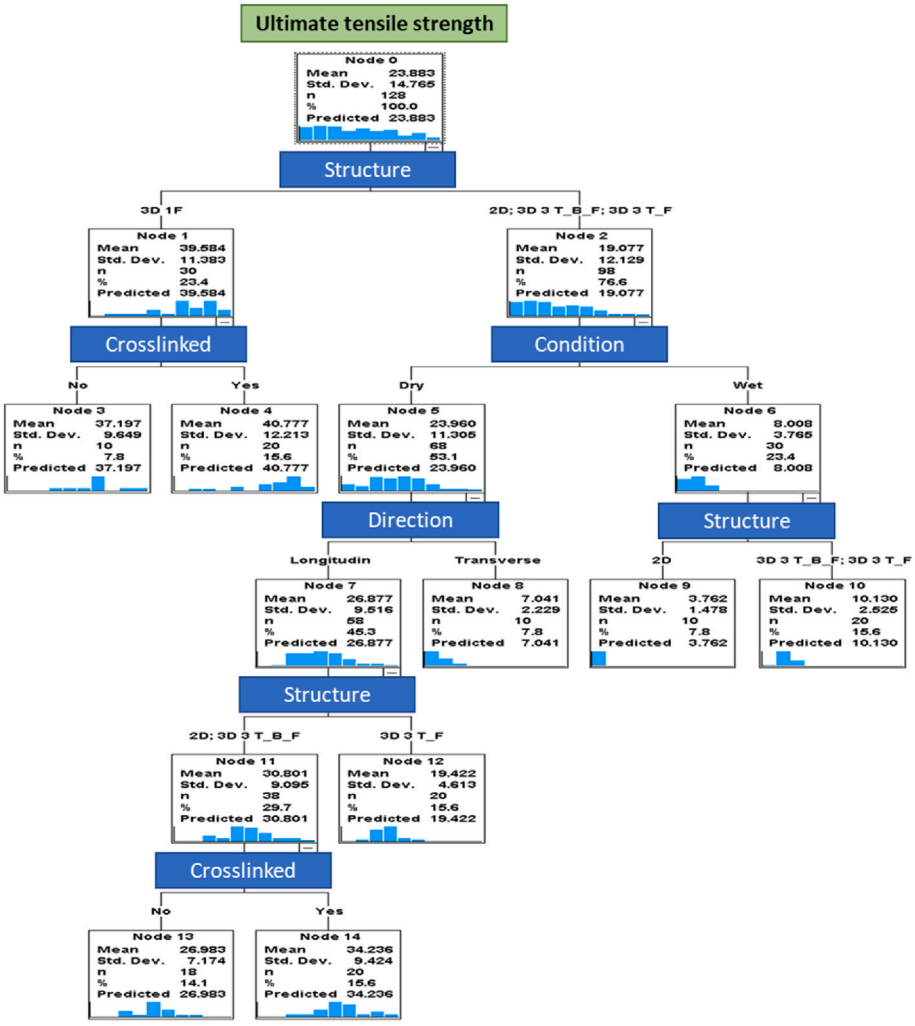

Fig. 7. CART for ultimate tensile strength.

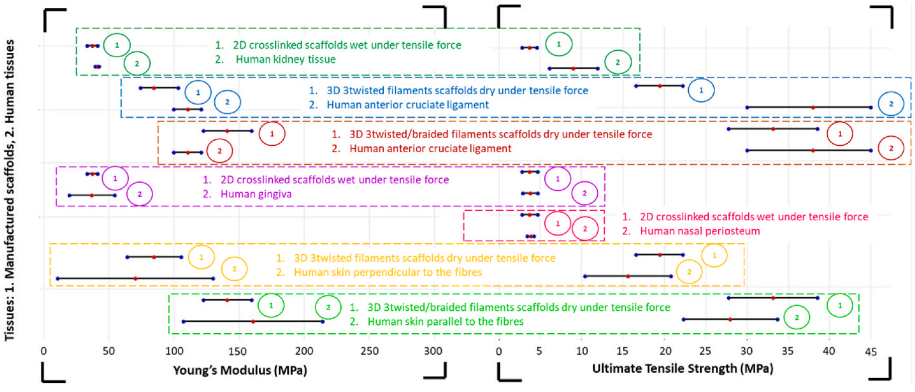

Fig. 8. Comparative between CART predictions and human tissues.

crosslinked 2D scaffolds tested under wet conditions; however, the predictions of the UTS were lower than the UTS of this human tissue.

4. Discussion

Traditional statistical and machine learning models were a powerful tool to predict the morphological and mechanical properties of electrospun scaffolds from different manufacturing conditions (Roldán et al., 2023a; Vatankhah et al., 2014). However, both techniques have different approaches. Whereas ML models provide the highest accuracy prediction in cases where the data is imbalanced, with nonlinear interactions or with non-parametric conditions (Roldán et al., 2023a; Bzdok et al., 2018b; Bzdok, 2017), statistical models are able to make inferential statements about the population (Bzdok and Ioannidis, 2019; Hunter and Holmes, 2023), find relationships between variables and assess models based on confidence intervals and significance test (Breiman, 2001) when parametric conditions are met and data is carefully collected and well-balanced (He et al., 2017). When the parametric

Table 5
Comparative between KNN, RF, CUBIST and SVM predictions and human tissues (Noyes and Grood, 1976; Choi et al., 2020; Joodaki and Panzer, 2018; Ottenio et al., 2015; Ní Annaidh et al., 2012; Snedeker et al., 2005; Zeng et al., 2003; Jansen and Rottier, 1958; Dunn and Silver, 1983; Butler et al., 1986; Siegler et al., 1988).

Native tissue and ML models		Young's Modulus (MPa)			Ultimate Tensile Strength (MPa)			Manufacturing levels factors
		YM Max	YM Mean	YM Min	UTS Max	UTS Mean	UTS Min	
Skin Parallel to the Langer lines	**Native**	**214.000**	**160.800**	**107.600**	**33.700**	**28.000**	**22.300**	**Condition (Dry) + Structure (3D 3T_B_F) + Crosslinked (Yes)**
	KNN	171.864	140.594	109.323	33.523	26.885	23.530	
	RF	170.712	156.572	142.432	30.793	27.755	24.717	
	SVM	162.488	153.419	144.350	32.497	29.541	26.586	
	Tune SVM	162.763	153.190	143.617	30.970	29.013	27.056	
	CUBIST	157.173	150.300	143.428	30.977	27.830	24.684	
	Tune CUB	157.173	154.113	146.513	31.017	27.674	24.332	
Skin Perpendicular to the Langer lines	**Native**	**130.100**	**70.600**	**11.100**	**20.800**	**15.600**	**10.400**	**Condition (Dry) + Structure (3D 3T_F) + Crosslinked (No)**
	KNN	86.018	82.984	79.951	18.263	17.922	17.465	
	RF	85.884	83.833	81.782	18.314	17.902	17.490	
	SVM	85.866	83.727	81.588	19.659	18.313	16.967	
	Tune SVM	85.877	83.747	81.617	19.660	18.315	16.969	
	CUBIST	87.998	84.572	81.147	18.263	17.864	17.465	
	Tune CUB	86.018	82.984	79.951	18.263	17.864	17.465	
Anterior cruciate ligament	**Native**	**121.000**	**111.000**	**100.000**	**45.000**	**38.000**	**30.000**	**Condition (Dry) + Structure (3D 3T_B_F) + Crosslinked (Yes)**
	KNN	171.864	140.594	109.323	40.018	38.159	37.602	
	RF	143.299	138.098	132.897	39.683	38.739	37.795	
	SVM	143.005	132.113	121.222	41.372	40.498	39.624	
	Tune SVM	143.044	132.135	121.227	40.946	39.344	37.742	
	CUBIST	147.909	133.222	118.536	39.982	38.777	37.573	
	Tune CUB	135.837	128.181	120.526	40.018	38.810	37.602	
Nasal cavity nasal periosteum	**Native**				**4.200**	**3.880**	**3.400**	**Condition (Wet) + Structure (2D) + Crosslinked (Yes)**
	KNN				4.090	3.762	3.504	
	RF				4.152	3.824	3.497	
	SVM				5.305	4.886	4.467	
	Tune SVM				4.784	4.327	3.870	
	CUBIST				4.090	3.797	3.504	
	Tune CUB				4.090	3.797	3.504	
Oral cavity Gingiva	**Native**	**54.760**	**37.360**	**19.960**	**4.710**	**3.810**	**2.910**	**Condition (Wet) + Structure (2D) + Crosslinked (Yes)**
	KNN	40.268	38.719	37.170	4.090	3.762	3.504	
	RF	42.400	40.292	38.185	4.152	3.824	3.497	
	SVM	49.265	47.673	46.080	5.305	4.886	4.467	
	Tune SVM	47.698	44.305	40.913	4.784	4.327	3.870	
	CUBIST	41.237	39.019	36.801	4.090	3.797	3.504	
	Tune CUB	41.198	39.210	37.223	4.090	3.797	3.504	
Kidney tissue	**Native**	43.000	41.500	40.000	11.900	9.000	6.100	**Condition (Wet) + Structure (2D) + Crosslinked (Yes)**
	KNN	40.268	38.719	37.170	4.090	3.762	3.504	
	RF	42.400	40.292	38.185	4.152	3.824	3.497	
	SVM	49.265	47.673	46.080	5.305	4.886	4.467	
	Tune SVM	47.698	44.305	40.913	4.784	4.327	3.870	
	CUBIST	41.237	39.019	36.801	4.090	3.797	3.504	
	Tune CUB	41.198	39.210	37.223	4.090	3.797	3.504	

conditions are not met, non-parametrical statistics such as Kruskal–Wallis and Mann–Whitney U tests or ML techniques can be applied.

This novel study explored the suitability of 28 ML models to understand the influence between variables and predict the mechanical properties (Young's modulus and ultimate tensile strength) of non-crosslinked and crosslinked 2D and 3D PVA-based scaffolds tested under various conditions, as well as investigate their suitability to identify the structures that best mimic human tissues.

Even though traditional parametrical statistics are used for inferential analysis and to establish relationships between variables, non-parametrical ML techniques are able to evaluate the importance of the exogenous variables on the endogenous variables. In this study, we demonstrated that the importance of the independent variables showed in CART models were in agreement with the regression coefficient calculated for LM, Step AIC, GAM and EARTH models, the Eta values calculated with the MANOVA and the average of the importance calculated with all the ML models. It was also demonstrated that the variables that contributed the most to the prediction of the Young's modulus were the "Structure" and the "Environmental condition", and the most important variables for the prediction of the UTS were "Environmental condition", "Structure" and "Direction". In all of the analysis, the variable with less influence on the prediction of the dependent variables was the "Crosslinked". These findings are meaningful since it will determine which aspects or variables should be further investigated to mimic more accurately the mechanical behaviour of human tissue, and which variables could be omitted. Due to the novelty of this study,

comparison with other publications could not be done to discuss these findings.

A key point in ML models is balancing the predictability and interpretability of the models. Linear models are able to provide the relationship between the predicted variable and its predictors through a first-degree polynomic equation, what makes them the easiest option to interpret the influences between the dependent variable and the independent variables. However, they require compliance with parametric conditions that sometimes are difficult to meet, and their predictability, assessed with the coefficient of determination and errors of the models, generally is lower than other models such as CART, RF or CUBIST models (Roldán et al., 2023a; Zhou et al., 2019). Two interactions can be added to these models to improve their predictability (R^2) by 25% (Molnar, 2019); however, this approach would complicate their interpretability. As with linear models, regression models such as GLM, Step AIC, GAM, GBM, EARTH and GLMNET had a relatively easy interpretability but a poor predictability. CART models were a very intuitive and powerful tool to understand the importance of the independent variables on the dependent one and interpret the predictions to be able to identify coincidences with human tissues. CART models marked the threshold between models which provided bad predictions (high MAPE and RMSE and low R^2) and non-parametric models that generated better predictions. KNN, RF, CUBIST and SVM presented the highest goodness of fit and lowest errors, especially CUBIST and SVM models with their optimised parameters. However, these models are known as "black-box" models that are difficult to interpret. This study assessed the predictions obtained with these non-parametric models and identifies six different situations where our scaffolds could be used as human tissue replacements for skin tissue, ligamentous tissue, gingival and nasal tissue, and renal tissue. It is noteworthy that this analysis is made possible because of the coefficient of determination and errors obtained with the test and with cross-validation were comparable. In some cases, such as with CUBIST and SVM models, predictions were better with test data than after cross-validation, this fact confirmed the replicability and reproducibility of the models. Traditional techniques for identifying possible human tissues will only study the mean and standard deviation of the scaffolds produced at a certain factor level, making it difficult to guarantee the reproducibility of the experiments and calculate errors.

Three main limitations are associated with this study. The first limitation is that only Young's modulus and ultimate tensile strength were explored in this study; therefore, once the potential human tissues are identified a deeper look at the mechanical performance of both the samples and the human tissues would be required to assess if the mechanical behaviour of the human tissue is fully mimicked by the samples and their testing conditions. The second limitation is associated with the calculation of the nominal cross-sectional area of the samples. In this study, three different techniques have been used to calculate the thickness of the 2D samples and the diameter of our 3D samples, a digital calliper, an analogue calliper and SEM images. Each technique has its limitations, for instance digital and analogue callipers can compress the samples and SEM images do not consider the topography of the sample. To minimise the errors, three measurements were taken for each sample and equipment, and the average was calculated to determine the thickness or diameter depending on the structure of the sample. Measurements from the same sample resulted in the same order of magnitude for the three techniques, demonstrating their correlation. Cross-sectional area of 2D samples were calculated with the width and average thickness of the sample and the nominal cross-sectional area of 3D samples were calculated with the average diameter of the samples. The third limitation is related to the number of observations, since a relatively small number of observations, 128 observations for each endogenous variable, informed the MANOVA and ML models, a larger dataset would improve the model's accuracy, increasing the coefficient of determination and reducing the errors. However, studies involving ML to predict mechanical properties reported similar and inferior number of observations, with 165 observations used to predict shear strength (Zhou et al., 2019), 60 observations were used to predict strain at break and ultimate tensile strength (Roldán et al., 2023a) or 16 observations were used to predict the elastic modulus (Vatankhah et al., 2014).

5. Conclusions

Traditional statistical models such as MANOVAs or linear regression models have demonstrated to be useful tools to predict the mechanical properties of electrospun scaffolds and establish relationships between the variables; however, when the parametrical conditions are not met or data presents complex non-linear interactions, more advanced statistics such as machine learning models have proved to be powerful predicted tools (Roldán et al., 2023a). Predictions provided from CART, KNN, RF, CUBIST and SVM models allowed the identification of six situations in which our structures tested under certain environmental and loading conditions were able to mimic the Young's modulus and ultimate tensile strength of human tissues such as kidney tissue, anterior cruciate ligament, gingiva, nasal periosteum and human skin tested perpendicular and parallel to the fibres. Although CART models were an innovative and easy to interpret tool to identify biomimetic electrospun structures, these models offered lower accuracy compared to less interpretable models such as CUBIST and SVM, which provided R^2 of 0.93 and 0.8 to predict the ultimate tensile strength and Young's modulus respectively. This novel approach can be implemented to optimise the manufacturing process in different applications and in particular, to build the basis for a further development of tissue engineered replacements.

Funding

This research received no external funding.

CRediT authorship contribution statement

Elisa Roldán: Writing – review & editing, Writing – original draft, Visualization, Validation, Project administration, Methodology, Investigation, Formal analysis, Data curation, Conceptualization. **Neil D. Reeves:** Writing – review & editing, Supervision, Resources. **Glen Cooper:** Writing – review & editing, Supervision, Resources. **Kirstie Andrews:** Writing – review & editing, Supervision, Resources.

Declaration of competing interest

The authors declare that they have no known competing financial interests or personal relationships that could have appeared to influence the work reported in this paper.

Data availability

Data will be made available on request.

Acknowledgments

Some experimental work included in this study was partially performed in the Manchester Institute of Biotechnology (University of Manchester). The authors would like to acknowledge Professor Paulo Jorge Da Silva Bartolo for his support allowing the use of the University of Manchester facilities. The authors would also like to thank the technical staff of the Manchester Metropolitan University, Mike Green for training ER on the use of the tensiometer.

Appendix A. Supplementary data

Supplementary data to this article can be found online at https://doi.org/10.1016/j.jmbbm.2024.106630.

References

Bancelin, S., Aimé, C., Gusachenko, I., Kowalczuk, L., Latour, G., Coradin, T., Schanne-Klein, M.-C., 2014. Determination of collagen fibril size via Absolute measurements of second-Harmonic generation Signals. Nat. Commun. 5 https://doi.org/10.1038/ncomms5920.

Bosworth, L.A., Alam, N., Wong, J.K., Downes, S., 2013. Investigation of 2D and 3D electrospun scaffolds Intended for tendon repair. J. Mater. Sci. Mater. Med. 24, 1605–1614. https://doi.org/10.1007/s10856-013-4911-8.

Breiman, L., 2001. Statistical modeling: the two cultures (with comments and a rejoinder by the author). Stat. Sci. 16, 199–231. https://doi.org/10.1214/ss/1009213726.

Butler, D.L., Kay, M.D., Stouffer, D.C., 1986. Comparison of material properties in fascicle-bone Units from human Patellar tendon and knee ligaments. J. Biomech. 19, 425–432. https://doi.org/10.1016/0021-9290(86)90019-9.

Bzdok, D., 2017. Classical statistics and statistical learning in imaging Neuroscience. Front. Neurosci. 11 https://doi.org/10.3389/fnins.2017.00543.

Bzdok, D., Ioannidis, J.P.A., 2019. Exploration, inference, and prediction in Neuroscience and Biomedicine. Trends Neurosci. 42, 251–262. https://doi.org/10.1016/j.tins.2019.02.001.

Bzdok, D., Altman, N., Krzywinski, M., 2018a. Statistics versus machine learning. Nat. Methods 15, 233–234. https://doi.org/10.1038/nmeth.4642.

Bzdok, D., Altman, N., Krzywinski, M., 2018b. Statistics versus machine learning. Nat. Methods 15, 233–234. https://doi.org/10.1038/nmeth.4642.

Chen, W., Xu, Y., Liu, Y., Wang, Z., Li, Y., Jiang, G., Mo, X., Zhou, G., 2019. Three-dimensional printed electrospun Fiber-based scaffold for Cartilage Regeneration. Mater. Des. 179, 107886 https://doi.org/10.1016/j.matdes.2019.107886.

Chen, Y., Shafiq, M., Liu, M., Morsi, Y., Mo, X., 2020a. Advanced fabrication for electrospun three-Dimensional nanofiber Aerogels and scaffolds. Bioact. Mater. 5, 963–979. https://doi.org/10.1016/j.bioactmat.2020.06.023.

Chen, W., Xu, Y., Li, Y., Jia, L., Mo, X., Jiang, G., Zhou, G., 2020b. 3D printing electrospinning Fiber-Reinforced Decellularized extracellular matrix for Cartilage Regeneration. Chem. Eng. J. 382, 122986 https://doi.org/10.1016/j.cej.2019.122986.

Choi, J.J.E., Zwirner, J., Ramani, R.S., Ma, S., Hussaini, H.M., Waddell, J.N., Hammer, N., 2020. Mechanical properties of human oral Mucosa tissues are site dependent: a combined Biomechanical, Histological and Ultrastructural approach. Clin Exp Dent Res 6, 602–611. https://doi.org/10.1002/cre2.305.

Doshi-Velez, F., Kim, B., 2017. Towards A Rigorous Science of Interpretable Machine Learning.

Dunn, M.G., Silver, F.H., 1983. Viscoelastic behavior of human Connective tissues: Relative contribution of Viscous and elastic Components. Connect. Tissue Res. 12, 59–70.

Freeman, J.W., Woods, M.D., Laurencin, C.T., 2007a. Tissue engineering of the anterior cruciate ligament using a Braid-Twist scaffold design. J. Biomech. 40, 2029–2036. https://doi.org/10.1016/j.jbiomech.2006.09.025.

Freeman, J.W., Woods, M.D., Laurencin, C.T., 2007b. Tissue engineering of the anterior cruciate ligament using a Braid-Twist scaffold design. J. Biomech. 40, 2029–2036. https://doi.org/10.1016/j.jbiomech.2006.09.025.

He, F., Mazumdar, S., Tang, G., Bhatia, T., Anderson, S.J., Dew, M.A., Krafty, R., Nimgaonkar, V., Deshpande, S., Hall, M., et al., 2017. Non-parametric MANOVA approaches for non-normal multivariate Outcomes with Missing values. Commun. Stat. Theor. Methods 46, 7188–7200. https://doi.org/10.1080/03610926.2016.1146767.

Hunter, D.J., Holmes, C., 2023. Where Medical statistics meets artificial Intelligence. N. Engl. J. Med. 389, 1211–1219. https://doi.org/10.1056/NEJMra2212850.

Jansen, L.H., Rottier, P.B., 1958. Some mechanical properties of human Abdominal skin measured on Excised Strips. DRM 117, 65–83. https://doi.org/10.1159/000255569.

Jiang, J., Carlson, M.A., Teusink, M.J., Wang, H., MacEwan, M.R., Xie, J., 2015. Expanding two-Dimensional electrospun nanofiber Membranes in the third Dimension by a Modified gas-foaming technique. ACS Biomater. Sci. Eng. 1, 991–1001. https://doi.org/10.1021/acsbiomaterials.5b00238.

Joodaki, H., Panzer, M.B., 2018. Skin mechanical properties and modeling: a review. Proc. Inst. Mech. Eng. H 232, 323–343. https://doi.org/10.1177/0954411918759801.

Joshi, M.K., Pant, H.R., Tiwari, A.P., kim, H.J., Park, C.H., Kim, C.S., 2015. Multi-layered Macroporous three-Dimensional nanofibrous scaffold via a novel gas foaming technique. Chem. Eng. J. 275, 79–88. https://doi.org/10.1016/j.cej.2015.03.121.

Kamolz, L.-P., Kotzbeck, P., Schintler, M., Spendel, S., 2022. Skin Regeneration, Repair, and Reconstruction: present and Future. Eur. Surg. 54, 163–169. https://doi.org/10.1007/s10353-022-00757-9.

Kuhn, M., 2008. Building predictive models in R using the caret package. J. Stat. Software 28, 1–26. https://doi.org/10.18637/jss.v028.i05.

Kuhn, M., Johnson, K., 2013. Applied Predictive Modeling. Springer, New York, NY, USA.

Kuhn, M., Weston, S., Keefer, C., Coulter, N., Quinlan, R., 2014. Cubist: rule-and instance-based regression modeling. R Package Version 0.0.18; CRAN: Vienna, Austria.

Laurencin, C.T., Freeman, J.W., 2005. Ligament tissue engineering: an Evolutionary materials science approach. Biomaterials 26, 7530–7536. https://doi.org/10.1016/j.biomaterials.2005.05.073.

Martin-Barragan, B., Lillo, R., Romo, J., 2014. Interpretable support Vector machines for functional data. Eur. J. Oper. Res. 232, 146–155. https://doi.org/10.1016/j.ejor.2012.08.017.

Miller, T., 2019. Explanation in artificial Intelligence: Insights from the Social Sciences. Artif. Intell. 267, 1–38. https://doi.org/10.1016/j.artint.2018.07.007.

Moeller, H.D., Bosch, U., Decker, B., 1995. Collagen fibril diameter distribution in Patellar tendon autografts after Posterior cruciate ligament Reconstruction in Sheep: changes over time. J. Anat. 187, 161–167.

Moharamzadeh, K., Colley, H., Murdoch, C., Hearnden, V., Chai, W.L., Brook, I.M., Thornhill, M.H., MacNeil, S., 2012. Tissue-engineered oral Mucosa. J. Dent. Res. 91, 642–650. https://doi.org/10.1177/0022034511435702.

Molnar, C., 2019. Interpretable Machine Learning. Lean Publishing.

Mouthuy, P.-A., Zargar, N., Hakimi, O., Lostis, E., Carr, A., 2015. Fabrication of continuous electrospun filaments with potential for Use as Medical fibres. Biofabrication 7. https://doi.org/10.1088/1758-5090/7/2/025006.

Muqeet, M., Malik, H., Panhwar, S., Khan, I.U., Hussain, F., Asghar, Z., Khatri, Z., Mahar, R.B., 2023. Enhanced cellulose nanofiber mechanical stability through ionic crosslinking and interpretation of adsorption data using machine learning. Int. J. Biol. Macromol. 237, 124180 https://doi.org/10.1016/j.ijbiomac.2023.124180.

Ní Annaidh, A., Bruyère, K., Destrade, M., Gilchrist, M.D., Otténio, M., 2012. Characterization of the Anisotropic mechanical properties of Excised human skin. J. Mech. Behav. Biomed. Mater. 5, 139–148. https://doi.org/10.1016/j.jmbbm.2011.08.016.

Noyes, F.R., Grood, E.S., 1976. The strength of the anterior cruciate ligament in humans and Rhesus Monkeys. J. Bone Joint Surg. Am. 58, 1074–1082.

Ottenio, M., Tran, D., Ní Annaidh, A., Gilchrist, M.D., Bruyère, K., 2015. Strain rate and Anisotropy effects on the tensile Failure characteristics of human skin. J. Mech. Behav. Biomed. Mater. 41, 241–250. https://doi.org/10.1016/j.jmbbm.2014.10.006.

Pedregosa, F., Varoquaux, G., Gramfort, A., Michel, V., Thirion, B., Grisel, O., Blondel, M., Prettenhofer, P., Weiss, R., Dubourg, V., et al., 2011. Scikit-learn: machine learning in Python. J. Mach. Learn. Res. 12, 2825–2830.

PyCaret available online. https://pycaret.org/. (Accessed 12 January 2024).

Rashid, S.T., Fuller, B., Hamilton, G., Seifalian, A.M., 2008. Tissue engineering of a Hybrid bypass graft for coronary and lower Limb bypass Surgery. Faseb. J. 22, 2084–2089. https://doi.org/10.1096/fj.07-096586.

Ribeiro, M.T., Singh, S., Guestrin, C., 2016. Model-Agnostic Interpretability of Machine Learning.

Roldán, E., Reeves, N.D., Cooper, G., Andrews, K., 2016. Design Consideration for ACL Implants based on mechanical loading. Procedia CIRP 49, 133–138. https://doi.org/10.1016/j.procir.2015.11.002.

Roldán, E., Reeves, N.D., Cooper, G., Andrews, K., 2017. In Vivo mechanical behaviour of the anterior cruciate ligament: a study of six Daily and high impact Activities. Gait Posture 58, 201–207. https://doi.org/10.1016/j.gaitpost.2017.07.123.

Roldán, E., Reeves, N.D., Cooper, G., Andrews, K., 2023a. Towards the ideal vascular implant: use of machine learning and statistical approaches to optimise manufacturing parameters. Front. Phys. 11 https://doi.org/10.3389/fphy.2023.1112218.

Roldan, E., Reeves, N., Cooper, G., Andrews, K., 2023a. Physiological mechanical testing and in-Vivo mechanical behaviour to inform the production of biomimetic tissue engineered ligaments. Tissue Eng. Part A 29. https://doi.org/10.1089/ten.tea.2023.29043.abstracts.

Roldan, E., Reeves, N., Cooper, G., Andrews, K., 2023b. Optimization of manufacturing parameters through machine learning techniques to create biomimetic vascular Implants. Tissue Eng. Part A 29. https://doi.org/10.1089/ten.tea.2023.29043.abstracts.

Roldán, E., Reeves, N.D., Cooper, G., Andrews, K., 2023b. Can We achieve biomimetic electrospun scaffolds with gelatin Alone? Front. Bioeng. Biotechnol. 11 https://doi.org/10.3389/fbioe.2023.1160760.

Roldán, E., Reeves, N.D., Cooper, G., Andrews, K., 2024. 2D and 3D PVA electrospun scaffold evaluation for ligament implant replacement: a mechanical testing, Modelling and experimental Biomechanics approach. Materialia, 102042. https://doi.org/10.1016/j.mtla.2024.102042.

Rothrauff, B.B., Lauro, B.B., Yang, G., Debski, R.E., Musahl, V., Tuan, R.S., 2017. Braided and Stacked electrospun nanofibrous scaffolds for tendon and ligament tissue engineering. Tissue Eng Part A 23, 378–389. https://doi.org/10.1089/ten.TEA.2016.0319.

Sensini, A., Gualandi, C., Cristofolini, L., Tozzi, G., Dicarlo, M., Gabriella, Teti, Mattioli-Belmonte, M., Focarete, M.L., 2017. Biofabrication of Bundles of Poly(Lactic Acid)-collagen Blends mimicking the Fascicles of the human Achille tendon. Biofabrication 9. https://doi.org/10.1088/1758-5090/aa6204.

Sensini, A., Santare, M.H., Eichenlaub, E., Bloom, E., Gotti, C., Zucchelli, A., Cristofolini, L., 2021. Tuning the structure of Nylon 6,6 electrospun Bundles to mimic the mechanical performance of tendon Fascicles. Front. Bioeng. Biotechnol. 9.

Shino, K., Oakes, B.W., Horibe, S., Nakata, K., Nakamura, N., 1995. Collagen fibril populations in human anterior cruciate ligament Allografts. Electron Microscopic analysis. Am. J. Sports Med. 23, 203–208. https://doi.org/10.1177/036354659502300213. ; discussion 209.

Si, Y., Wang, X., Yan, C., Yang, L., Yu, J., Ding, B., 2016. Ultralight Biomass-Derived Carbonaceous nanofibrous Aerogels with Superelasticity and high Pressure-Sensitivity. Adv. Mater. 28, 9512–9518. https://doi.org/10.1002/adma.201603143.

Siegler, S., Block, J., Schneck, C.D., 1988. The mechanical characteristics of the Collateral ligaments of the human Ankle Joint. Foot Ankle 8, 234–242. https://doi.org/10.1177/107110078800800502.

Smola, A.J., Schölkopf, B., 2004. A Tutorial on support Vector regression. Stat. Comput. 14, 199–222. https://doi.org/10.1023/B:STCO.0000035301.49549.88.

Snedeker, J.G., Niederer, P., Schmidlin, F.R., Farshad, M., Demetropoulos, C.K., Lee, J.B., Yang, K.H., 2005. Strain-rate dependent material properties of the Porcine and human kidney Capsule. J. Biomech. 38, 1011–1021. https://doi.org/10.1016/j.jbiomech.2004.05.036.

Strocchi, R., De Pasquale, V., Facchini, A., Raspanti, M., Zaffagnini, S., Marcacci, M., 1996. Age-related changes in human anterior cruciate ligament (ACL) collagen fibrils. Ital. J. Anat Embryol. 101, 213–220.

Sun, B., Long, Y.Z., Zhang, H.D., Li, M.M., Duvail, J.L., Jiang, X.Y., Yin, H.L., 2014. Advances in three-Dimensional nanofibrous Macrostructures via electrospinning. Prog. Polym. Sci. 39, 862–890. https://doi.org/10.1016/j.progpolymsci.2013.06.002.

Vatankhah, E., Semnani, D., Prabhakaran, M.P., Tadayon, M., Razavi, S., Ramakrishna, S., 2014. Artificial neural network for modeling the elastic modulus of electrospun polycaprolactone/gelatin scaffolds. Acta Biomater. 10, 709–721. https://doi.org/10.1016/j.actbio.2013.09.015.

Webb, C.W.B., D'Costa, K., Tawagi, E., Antonyshyn, J., Hofer, O.P.S., Santerre, J.P., 2023. Electrospun Methacrylated natural/Synthetic Composite Membranes for gingival tissue engineering. Acta Biomater. https://doi.org/10.1016/j.actbio.2023.11.021.

Yagli, G.M., Yang, D., Srinivasan, D., 2019. Automatic hourly solar Forecasting using machine learning models. Renew. Sustain. Energy Rev. 105, 487–498. https://doi.org/10.1016/j.rser.2019.02.006.

Zeng, Y.-J., Sun, X., Yang, J., Wu, W., Xu, X., Yan, Y., 2003. Mechanical properties of nasal Fascia and periosteum. Clin. Biomech. 18, 760–764. https://doi.org/10.1016/s0268-0033(03)00136-0.

Zhou, J., Li, E., Wei, H., Li, C., Qiao, Q., Armaghani, D.J., 2019. Random Forests and cubist algorithms for predicting shear strengths of Rockfill materials. Appl. Sci. 9, 1621. https://doi.org/10.3390/app9081621.